

Quantifying memory in spin glasses

I. Paga,^{1,*} J. He,^{2,†} M. Baity-Jesi,³ E. Calore,⁴ A. Cruz,^{5,6} L.A. Fernandez,⁷ J.M. Gil-Narvion,⁶
 I. Gonzalez-Adalid Pemartin,⁷ A. Gordillo-Guerrero,^{8,9} D. Iñiguez,^{6,10,5} A. Maiorano,^{11,6}
 E. Marinari,¹² V. Martin-Mayor,⁷ J. Moreno-Gordo,^{6,5,13,9} A. Muñoz Sudupe,⁷ D. Navarro,¹⁴
 R.L. Orbach,¹⁵ G. Parisi,¹² S. Perez-Gavero,^{5,6} F. Ricci-Tersenghi,¹² J.J. Ruiz-Lorenzo,^{13,9}
 S.F. Schifano,¹⁶ D.L. Schlagel,¹⁷ B. Seoane,^{18,6} A. Tarancon,^{5,6} and D. Yllanes^{19,6,20,21}

(Janus Collaboration)

¹*Department of Computing Sciences, Bocconi University, 20136 Milano, Italy*

²*Department of Mechanical Engineering, The University of Texas at Austin, Austin, Texas 78712, USA*

³*Eawag, Überlandstrasse 133, CH-8600 Dübendorf, Switzerland*

⁴*Dipartimento di Fisica e Scienze della Terra, Università di Ferrara e INFN, Sezione di Ferrara, I-44122 Ferrara, Italy*

⁵*Departamento de Física Teórica, Universidad de Zaragoza, 50009 Zaragoza, Spain*

⁶*Instituto de Biocomputación y Física de Sistemas Complejos (BIFI), 50018 Zaragoza, Spain*

⁷*Departamento de Física Teórica, Universidad Complutense, 28040 Madrid, Spain*

⁸*Departamento de Ingeniería Eléctrica, Electrónica y Automática, U. de Extremadura, 10003, Cáceres, Spain*

⁹*Instituto de Computación Científica Avanzada (ICCAEx),
Universidad de Extremadura, 06006 Badajoz, Spain*

¹⁰*Fundación ARAID, Diputación General de Aragón, Zaragoza, Spain*

¹¹*Dipartimento di Biotecnologie, Chimica e Farmacia,
Università degli studi di Siena, 53100, Siena Italy*

¹²*Dipartimento di Fisica, Sapienza Università di Roma, and CNR-Nanotec,
Rome Unit, and INFN, Sezione di Roma1, 00185 Rome, Italy*

¹³*Departamento de Física, Universidad de Extremadura, 06006 Badajoz, Spain*

¹⁴*Departamento de Ingeniería, Electrónica y Comunicaciones and I3A, U. de Zaragoza, 50018 Zaragoza, Spain*

¹⁵*Texas Materials Institute, The University of Texas at Austin, Austin, Texas 78712, USA*

¹⁶*Dipartimento di Scienze dell'Ambiente e della Prevenzione Università
di Ferrara and INFN Sezione di Ferrara, I-44122 Ferrara, Italy*

¹⁷*Division of Materials Science and Engineering, Ames Laboratory, Ames, Iowa 50011, USA*

¹⁸*Université Paris-Saclay, CNRS, INRIA Tau team, LISN, 91190 Gif-sur-Yvette, France*

¹⁹*Fundación ARAID, Diputación General de Aragón, Zaragoza, Spain*

²⁰*Zaragoza Scientific Center for Advanced Modeling (ZCAM), 50018 Zaragoza, Spain*

²¹*Chan Zuckerberg Biohub, San Francisco, CA, 94158*

(Dated: February 13, 2025)

Rejuvenation and memory, long considered the distinguishing features of spin glasses, have recently been proven to result from the growth of multiple length scales. This insight, enabled by simulations on the Janus II supercomputer, has opened the door to a quantitative analysis. We combine numerical simulations with comparable experiments to introduce two coefficients that quantify memory. A third coefficient has been recently presented by Freedberg et al. We show that these coefficients are physically equivalent by studying their temperature and waiting-time dependence.

Memory is among the most striking features of far-from-equilibrium systems [1], including granular materials [2], phase separation in the early universe [3] and, particularly, glass formers [4–10]. Whether a universal mechanism is responsible for memory in all these materials is unknown, but spin glasses stand out [11–17]. On the one hand, memory effects are particularly strong in these systems —perhaps because of the large attainable coherence lengths [18–20]. More importantly, their dynamics is now understood in great detail. Indeed, to model protocols where temperature is varied, one must first understand the nonequilibrium evolution at constant temperature. In other words, before tackling memory,

rejuvenation and aging should be mastered. These intermediate steps, including the crucial role of temperature chaos, have now been taken for spin glasses [21–23].

In the context of spin glasses, rejuvenation is the observation that when the system is aged at a temperature T_1 for a time t_{w1} , and then cooled to a sufficiently lower T_2 , the spin glass reverts apparently to the same state it would have achieved had it been cooled directly to T_2 . That is, its apparent state is independent of its having approached equilibrium at temperature T_1 . However, when the spin glass is then warmed back to temperature T_1 , it appears to return to its aged state, hence memory.

Conventional wisdom has long ascribed rejuvenation to temperature chaos —the notion that equilibrium states at close temperatures are unrelated— and memory was experimentally exhibited long ago [11, 12] but these effects remained unassailable to numerical simulations in three-dimensional systems [24–29]. This state of affairs

* ilaria.paga@gmail.com

† This author performed the experiments reported in this work.

has recently changed [30], thanks to the combination of multiple advances: the availability of the Janus II supercomputer [31] and of single-crystal experiments [18], accessing much larger coherence lengths; the establishment of a relation between experimental and numerical time scales [19, 20]; and the quantitative modelling of nonequilibrium temperature chaos [22]. Ref. [30] has not only demonstrated memory numerically and related rejuvenation to temperature chaos, but also shown that both effects are ruled by multiple length scales, setting the stage for a more quantitative study.

Here we introduce two coefficients to quantify memory, one experimentally accessible and the other adapted to numerical work. The example of temperature chaos has shown that such indices are key to a comprehensive theory [32–34]. In principle, the only constraints for such a coefficient \mathcal{C} are that $\mathcal{C} = 1$ means perfect memory and $\mathcal{C} = 0$ means that the memory has been totally erased. Many choices could satisfy these conditions: besides the coefficients introduced herein, [35] presents an alternative based on a different observable. Fortunately, the length scales discussed in [30] allow us to express these coefficients as smooth functions of similar scaling parameters and to demonstrate that they have the same physics as temperature and waiting time are varied.

Protocols. In both experiment and simulations [36], we have a three-step procedure: (i) the system is quenched to an aging temperature $T_1 < T_g$ (T_g is the glass temperature) and relaxes for a time t_{w1} . In simulations, this quench is instantaneous, while in experiment, it is done at ≈ 10 K/min. A protocol where T is kept constant after the initial quench is termed native. (ii) The system is then quenched to $T_2 < T_1$, where it evolves for time t_{w2} . (iii) The system is raised back to T_1 , instantaneously in simulations, and at the same rate as cooling in experiment. After a short time at T_1 (2^{10} time steps in simulations), the dynamics are compared to the native system, which has spent t_{w1} at T_1 . The temperature drop $T_1 - T_2$ is chosen to ensure that temperature chaos (and, hence, rejuvenation) is sizeable [23, 30]. Our experiments are performed on a sample with $T_g = 41.6$ K. For experimental parameters see Table I (Table II for simulations).

Length scales. Memory and rejuvenation are ruled by several related length scales [37], of which only one is experimentally accessible — ξ_{Zeeman} , related to the Zeeman effect [38]. In simulations, the basic length is the size of glassy domains in a native protocol, $\xi_{\text{micro}}^{\text{native}}$.

We regard rejuvenation as a consequence of temperature chaos. If the temperature drop meets the chaos requirement, namely the chaos length scale set by $T_1 - T_2$ is small compared to $\xi_{\text{micro}}^{\text{native}}(T_1, t_{w1})$ [23, 30], the system that has aged at the starting temperature T_1 for t_{w1} “rejuvenates” at the cold temperature T_2 . That is, preexisting correlated spins are “frozen” dynamically at T_2 and a new correlated state of size $\zeta(T_2, t_{w2})$ forms, where t_{w2} is the waiting time at T_2 . The newly created correlated state at T_2 is independent from that formed at T_1 .

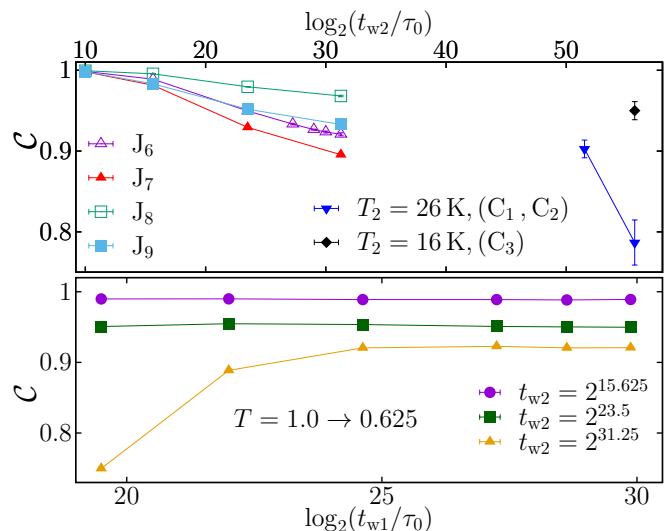


FIG. 1. **Memory coefficient** as a function of t_{w1} and t_{w2} . Top: Memory loss as a function of time t_{w2} both for our experiments (Table I) and for our simulations (Table II). The “natural” timescale τ_0 is 1.86×10^{-13} seconds for the experimental data and 1 lattice sweep for simulations. Bottom: Memory coefficient for fixed t_{w1} [fixed $\xi_{\text{micro}}(T_1, t_{w1})$] and several t_{w2} .

Protocol	T_1 (K)	t_{w1} (h)	T_2 (K)	t_{w2} (h)	T_m (K)	ξ/a
N ₁	30	1	—	—	30	13.075
N ₂	26	1/6	—	—	26	8.1011
N ₃	26	3	—	—	26	11.961
N ₄	16	3	—	—	16	6.3271
R ₁	30	1	26	3	26	11.787
C ₁	30	1	26	1/6	30	12.621
C ₂	30	1	26	3	30	12.235
C ₃	30	1	16	3	30	12.846

TABLE I. **Parameters of our experiments.** We use the abbreviations N (native), R (rejuvenation) and C (cycle), see paragraph *Protocols* for discussion. Unlike in rejuvenation protocols, in temperature cycles the temperature is brought back to T_1 before measurements start. We indicate the measuring temperature T_m , and —whenever possible— the value of ξ , in units of the average distance between nearest-neighbour spins. Measurements start after t_{w1} for native protocols ($t_{w1} + t_{w2}$ for cycle or rejuvenation protocols). The data for N₂ were taken at small values of H because non-linear effects enter for larger values of H at small t_w .

As t_w increases at T_2 , the newly correlated state at T_2 grows larger, to a maximum size set by the final time at T_2 , t_{w2} . Upon heating back to T_1 , the two correlated states *interfere*, causing a memory loss that will be seen both in experiment and simulations.

Simulations can easily access $\xi_{\text{micro}}^{\text{native}}$ and ζ [21, 30, 39, 40]. Experiments measure instead the number of correlated spins N_c [38]. Equivalently, in simulations, the native protocol results in

$$N_c^{\text{native}}(T, t_w) = [\xi_{\text{micro}}^{\text{native}}(T, t_w)]^{D-\theta/2}, \quad (1)$$

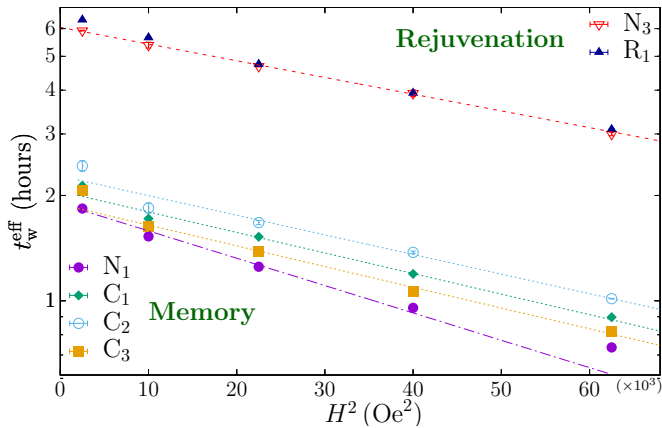


FIG. 2. **Rejuvenation** (top) and **memory** (bottom), as studied through the Zeeman-effect method of Ref. [38] on a single crystal of CuMn. Our thermal protocols are described in Tab. I. We show t_w^{eff} vs H^2 in logarithmic scale [$t_w^{\text{eff}}(H)$ is the time at which $S(t, H) = H^{-1}dM/d\log t$ peaks]. The number of correlated spins N_c for a given protocol is proportional to the slope of the corresponding curve. The values of t_w^{eff} essentially coincide for native protocol N_3 and for rejuvenation protocol R_1 at $T_2 = 26$ K (the previous relaxation at $T_1 = 30$ K undergone in protocol R_1 turns out to be irrelevant at 26 K). As for the memory coefficient, see Eq. (2), the slope of native protocol N_1 is approached either by decreasing the relaxation time t_{w2} at fixed T_2 (compare cycles C_1 and C_2) or by lowering T_2 at fixed t_{w2} (compare cycles C_2 and C_3).

where θ is the replicon exponent [19, 20, 36, 41]. If the chaos condition is met, and only in this case, the jump protocol results in, concomitantly, $N_c^{\text{jump}}(T_2, t_{w2}) \propto [\zeta(T_2, t_{w2})]^{D-\theta/2}$. Therefore, when chaos is strong enough, we have a dictionary relating the experimentally accessible N_c to these two basic length scales [30] (see also SM).

Qualitative behavior of the memory coefficient. According to the above, one would expect memory to depend on the ratio $\zeta(T_2, t_{w2})/\xi_{\text{micro}}^{\text{native}}(T_1, t_{w1})$: the smaller the ratio, the larger the memory. Because both lengths are increasing functions of time, then (i) memory should increase with increasing t_{w1} , everything else held constant. Concomitantly, (ii) memory should decrease with increasing t_{w2} , everything else held constant. Finally, (iii) if $\Delta T = T_1 - T_2$ increases, everything else held constant, $\zeta(T_2, t_{w2})$ will progressively decrease, and memory should increase. The memory coefficients that we define below, plotted in Fig. 1, display precisely these predicted variations. The experimental data in Fig. 1 agree with this expectation, which we shall test in our simulations through a scaling analysis.

Experimental definition of the memory coefficient. We define a memory coefficient from the number of correlated spins N_c , see Eq. (1). We shall first show that rejuvenation can be observed from N_c , thus confirming that temperature chaos is strong enough given our choice of temperatures and waiting times.

A small sample was cut from a single crystal of CuMn,

7.92 at.%, with $T_g = 41.6$ K. T_1 and t_{w1} in Table I were chosen to facilitate direct comparison with the results of Freedberg et al. [35], who defined another memory coefficient from the linear magnetic susceptibility. The lower temperature, T_2 , was variable, as was the waiting time t_{w2} . Our measurements of N_c follows Ref. [38] and are illustrated in Fig. 2–top. For the reader’s convenience, we briefly recall the main steps leading to the measurement of N_c (see Supplemental Material [url] for further details).

After the sample has undergone the appropriate preparatory protocol, we probe its dynamic state by switching on a magnetic field. We set time $t = 0$ when the field is switched on and record the magnetization $M(t)$, which grows steadily from $M(t = 0) = 0$, to obtain the dynamic response function $S(t, H) = H^{-1}dM/d\log t$. For native protocols and $H \rightarrow 0$, the peak of $S(t)$ against t occurs approximately at the effective time $t_w^{\text{eff}} \approx t_{w1}$. As H increases, the peak moves to shorter $t_w^{\text{eff}}(H)$. The slope of the plot of $\log t_w^{\text{eff}}$ vs H^2 equals the product of N_c times the field-cooled susceptibility per spin: $(\chi_{\text{FC}}/\text{spin})N_c - \chi_{\text{FC}}$ is roughly constant over the measured temperature range. We thus gain access to N_c .

We compare in Fig. 2–top the outcome of the above measuring procedure as obtained in protocols N_3 and R_1 (see Table I). The two systems evolve for the same time at 26 K. The values obtained for $\log t_w^{\text{eff}}$ turned out to be nearly identical: relaxation at 30 K does not leave measurable traces at 26 K, hence rejuvenation.

To quantify memory, we compare N_c for systems that have undergone the temperature-cycling protocols in Table I with their native counterparts. These measurements are illustrated in Fig. 2–bottom. We define the Zeeman-effect memory coefficient as

$$C_{\text{Zeeman}} = N_c^{\text{cycle}}/N_c^{\text{native}}. \quad (2)$$

Note that in both cases measurements are carried out at T_1 (the difference lies in the previous thermal history of the sample), hence the ratio in Eq. (2) is just the ratio of the corresponding slopes in Fig. 2–bottom. Our results for C_{Zeeman} are given in Fig. 1.

A memory coefficient from simulations. We extend [30] to quantify memory through a computation at the verge of current capabilities [42]. We look for memory through the quantity that can be extracted most accurately from simulations: the spin-glass correlation function at $H = 0$, $G_{\text{R}}(\mathbf{r}, t; p) = \overline{\langle q^{(a,b)}(\mathbf{x}, t)q^{(a,b)}(\mathbf{x} + \mathbf{r}, t) \rangle_p}$. Here, $q^{(a,b)}(\mathbf{x}, t) \equiv \sigma^{(a)}(\mathbf{x}, t)\sigma^{(b)}(\mathbf{x}, t)$ where (a, b) label different real replicas and $\langle \dots \rangle_p$ stands for the thermal average after a temperature cycle built from T -drop p (see Table II and Protocols) [43].

Our starting observation is that the experimental determination of C , Fig. 2, relies on the nonlinear response to the magnetic field. Interestingly enough, the equilibrium nonlinear susceptibility is proportional to the integral of $r^2 G_{\text{R}}$ with $r \in (0, \infty)$. Thus, following [19, 20, 41, 44], we generalize this equilibrium relation

T -drop	T_1	T_2	t_{w1}	$\xi_{\text{micro}}(T_1, t_{w1})$
J ₁	1.0	0.625	$2^{19.5}$	8.038(1)
J ₂	1.0	0.625	2^{22}	10.085(15)
J ₃	1.0	0.625	$2^{24.625}$	12.75(3)
J ₄	1.0	0.625	$2^{27.25}$	16.04(3)
J ₅	1.0	0.625	$2^{28.625}$	18.08(5)
J ₆	1.0	0.625	$2^{29.875}$	20.20(8)
J ₇	1.0	0.7	$2^{29.875}$	20.20(8)
J ₈	0.9	0.5	$2^{31.25}$	16.63(5)
J ₉	0.9	0.7	$2^{31.25}$	16.63(5)

TABLE II. **Building blocks (T -drop) for temperature cycles in our simulation.** The initially disordered system relaxes for a time t_{w1} at temperature T_1 , reaching a coherence length $\xi_{\text{micro}}(T_1, t_{w1})$. A T -drop is given by (T_1, T_2, t_{w1}) . To specify a temperature cycle one needs in addition t_{w2} , see the *Protocols* paragraph. Only J₉ does not meet the requirements for temperature chaos [30].

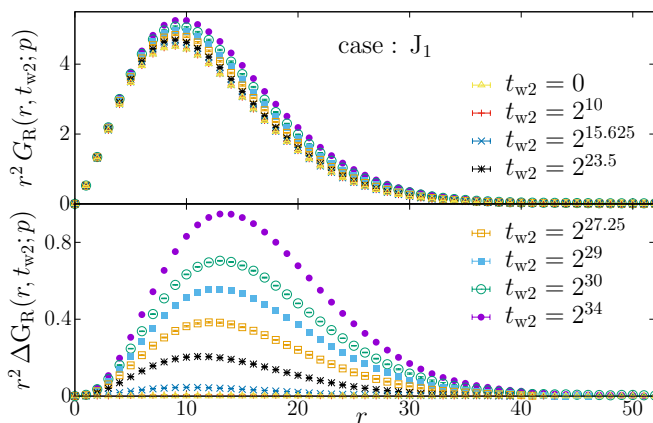


FIG. 3. **Numerical construction of a memory coefficient.** Top: the curves $r^2 G_R(r, t_{w2}; p)$ vs. r show small, but detectable, differences as t_{w2} varies, for temperature cycles built from the T -drop J₁ in Table II ($t_{w1} = 2^{19.5}$). Bottom: as in Top, but subtracting the native G_R from the correlation function of the temperature-cycled system. As the time spent at the colder temperature T_2 increases, the system loses memory. The memory loss is evinced by the increasing signal in $r^2 \Delta G_R$.

by computing these integrals using the nonequilibrium correlation function G_R .

Fig. 3-top exhibits a small but detectable difference in the behavior of $r^2 G_R$ as t_{w2} varies in cycles built from T -drop J₁ in Table II. This success has encouraged to consider the curve with $t_{w2} = 0$ as the reference curve [45]. We evaluate effects due to t_{w2} as $\Delta G_R(r, t_{w2}; p) = G_R(r, t_{w2}; p) - G_R(r, 0; p)$. ΔG_R measures the effects caused by aging at T_2 for a waiting time t_{w2} . If $T_1 - T_2$ is sufficient for full chaos to develop at T_2 , then $\Delta G_R(r, t_{w2}; T_1)$ represents the competing correlation length that interferes with the native correlation length established at T_1 .

From Fig. 3-bottom, it is natural to define the numer-

ical memory coefficient \mathcal{C}_{num} as

$$\mathcal{C}_{\text{num}} = 1 - \frac{\int_0^\infty dr r^2 \Delta G_R(r, t_{w2}; p)}{\int_0^\infty dr r^2 G_R(r, 0; p)}. \quad (3)$$

Given the accuracy we achieve for $\Delta G_R(r, t_{w2}; p)$, \mathcal{C}_{num} is sensitive to even tiny differences in the state of the system just before and just after the temperature cycle. Some scaling relations linking \mathcal{C}_{num} , $\mathcal{C}_{\text{Zeeman}}$ and the coefficient proposed in Ref. [35] are discussed in the Supplemental Material [url] which includes also Refs.[46, 47]. Our results for \mathcal{C}_{num} are presented in Fig. 1, for several temperature cycles built from the temperature drops in Table II. The values of T_1 , T_2 and t_{w1} were chosen to meet the chaos requirement proposed in [23, 30] (the only exception is J₉, used as a testing case for the scaling analysis, below). It is comforting that, even when the ratio t_{w2}/t_{w1} is as large as in Fig. 3, we still obtain $\mathcal{C}_{\text{num}} > 0.75$.

Discussion. Memory can be quantified in several ways: we have proposed two such memory coefficients, $\mathcal{C}_{\text{Zeeman}}$ and \mathcal{C}_{num} , respectively, adapted to experimental and numerical computation. Each coefficient is used in a different time scale, see Fig. 1. Furthermore, [35] proposes yet another experimental coefficient, $\mathcal{C}_{\chi''}$, based on the linear response to a magnetic field (rather than the nonlinear responses considered herein). It is obvious that more options exist. Hence, it is natural to ask what (if any) is the relationship between these coefficients.

We look for this relationship in the two length scales that rule our nonequilibrium dynamics, namely $\zeta(T_2, t_{w2})$ and $\xi_{\text{micro}}^{\text{native}}(T_1, t_{w1})$. If we succeed in expressing our coefficients as simple functions of these two lengths, we shall naturally link different memory definitions.

Specifically, we consider two variables x and y :

$$x = \left[\frac{\zeta(T_2, t_{w2})}{\xi_{\text{micro}}^{\text{native}}(T_1, t_{w1})} \right]^{D-\theta/2}, \quad y = \frac{T_1}{T_g} \zeta(T_2, t_{w2}). \quad (4)$$

Both scaling variables, x and y , are approximately accessible to experiment through N_c^{jump} and N_c^{native} ; we shall name their experimental proxies x' and y' [48]. Therefore, we seek numerical constants a_1 and a_2 , [see SM for details], such that the \mathcal{C}_{num} from all our temperature cycles fall onto a single function of

$$\mathcal{F}(x, y) = y [1 + a_1 x + a_2 x^2]. \quad (5)$$

Setting aside T -drop J₉, which does not meet the chaos condition, the overall linear behavior in Fig. 4-bottom is reassuring.

With appropriate a'_1 and a'_2 in Eq. (5), see SM for details, the data for $\mathcal{C}_{\chi''}$ [35] also fall onto a smooth function of $\mathcal{F}'(x', y')$, Fig. 4-top. There is a problem, however: $\mathcal{C}_{\chi''}$ goes to one for t_{w2} significantly larger than zero ($\mathcal{F}' = 0$ only at $t_{w2} = 0$). The same problem afflicts \mathcal{C}_{num} , albeit to a lesser degree. Interestingly, when plotted as a function of \mathcal{F}' , $\mathcal{C}_{\text{Zeeman}}$ is compatible with a straight line that goes through $\mathcal{C} = 1$ at $\mathcal{F}' = 0$, as it should. So, at least in this respect, $\mathcal{C}_{\text{Zeeman}}$ is the most sensible coefficient.

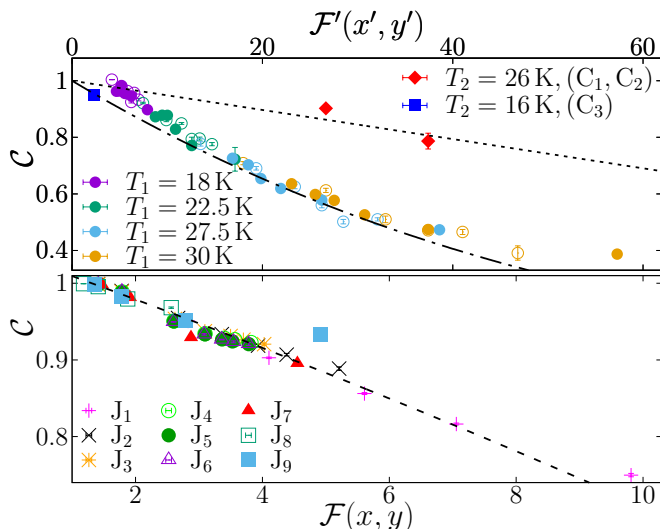


FIG. 4. Top: Experimental memory coefficients $C_{\chi''}$ (circles, data from [35]; $T_1 = T_2 + 4$ K) and C_{Zeeman} (rhombus and squares, see Table I) versus the scaling function in Eq. (5). See text for the computation of the x' and y' proxies. Empty circles refer to $t_{w1} = 1$ h (full circles for $t_{w2} = 3$ h). The dotted line is a fit to a straight $C_{\text{Zeeman}} = 1 - \alpha \mathcal{F}'$. The dashed line is $(1 - \alpha \mathcal{F}')^{3.9}$ and represents the experimental findings for $C_{\chi''}$ surprisingly well. Bottom: As in Top, for memory coefficient C_{num} [x and y are given in Eq. (4)], see Table II for details.

Perhaps more importantly, the scaling representation (dashed line in Fig. 4–top) evinces that, away from the $C \approx 1$ region, the relation $C_{\chi''} \approx [C_{\text{Zeeman}}]^K$ holds with $K \approx 3.9$. This relation makes it obvious that the different memory coefficients carry the same physical information. Although the scaling in Eq. (5) could be feared to be accurate only near $C \approx 1$, we have been lucky: our ansatz turns out to cover all reachable values of C .

In summary, we have developed a quantitative formulation for memory in rejuvenated glasses utilizing measured and calculated coherence lengths. In combination, they account quantitatively for memory from experiment and simulations. We have confirmed that rejuvenation and temperature chaos are strongly related effects [30]. Our results are based on first principles without the need for extraneous parameters. Our approach is easily extended to the many other glassy systems that exhibit these phenomena.

ACKNOWLEDGMENTS

We are grateful for helpful discussions with S. Swinnea about sample characterization. We thank J. Freedberg and coauthors for sharing their data and letting us analyze them. This work was partially supported by the U.S. Department of Energy, Office of Basic Energy Sciences, Division of Materials Science and Engineering, under Award No. DE-SC0013599. Crystal growth of the Cu0.92Mn0.08 sample was performed by

Deborah L. Schlager at the Materials Preparation Center, Ames National Laboratory, U.S. Department of Energy, and supported by the Department of Energy, Basic Energy Sciences, under Contract No. DE-AC02-07CH11358. We were partly funded as well by Grant No. PID2022-136374NB-C21, PID2022-136374NB-C22, PID2020-112936GB-I00, PID2019-103939RB-I00, PGC2018-094684-B-C22 and PID2021-125506NA-I00, funded by Ministerio de Ciencia, Innovación y Universidades (Spain), Agencia Estatal de Investigación (AEI, Spain, 10.13039/501100011033), and European Regional Development Fund (ERDF, A way of making Europe). We were also partly funded by the DGA-FSE (Diputación General de Aragón—Fondo Social Europeo). This research has been supported by the European Research Council under the European Unions Horizon 2020 research and innovation program (Grant No. 694925—Lotglassy, G. Parisi) and by ICSC—Centro Nazionale di Ricerca in High Performance Computing, Big Data, and Quantum Computing funded by European Union—NextGenerationEU, and the FIS 2021 funding scheme (FIS783—SMaC), and by the PRIN funding scheme (2022LMHTET—Complexity) both from Italian MUR. IGAP was supported by the Ministerio de Ciencia, Innovación y Universidades (MCIU, Spain) through FPU Grant No. FPU18/02665. IP was supported by LazioInnova—Regione Lazio under the program Gruppi di ricerca 2020—POR FESR Lazio 2014-2020, Project NanoProbe (Application code A0375-2020-36761)

Appendix A: Our simulations on Janus II

We simulate the Edwards-Anderson model in a cubic lattice with linear size $L = 160$ and periodic boundary conditions. The Ising spins $S_{\mathbf{x}} = \pm 1$ occupy the lattice nodes and interact with their nearest lattice-neighbors through the Hamiltonian

$$H = - \sum_{\langle \mathbf{x}, \mathbf{y} \rangle} J_{\mathbf{x}, \mathbf{y}} S_{\mathbf{x}} S_{\mathbf{y}}, \quad (\text{A1})$$

where the coupling constants are independent random variables that are fixed at the beginning of the simulation (we choose $J_{\mathbf{x}, \mathbf{y}} = \pm 1$ with 50% probability). A choice of the $\{J_{\mathbf{x}, \mathbf{y}}\}$ is named a sample. The model in Eq. (A1) undergoes a phase transition at temperature $T_c = 1.1019(29)$ [49], separating the paramagnetic phase (at high temperatures) from the spin-glass phase (at low temperatures).

We study the nonequilibrium dynamics of the model with a Metropolis algorithm. The time unit is a full lattice sweep (roughly corresponding to one picosecond of physical time [50]). The simulation is performed on the Janus II custom-built supercomputer [31]

We consider 16 statistically independent samples. For each sample, we simulate $N_R = 512$ independent replicas (*i.e.*, N_R system copies that share the couplings $\{J_{\mathbf{x}, \mathbf{y}}\}$)

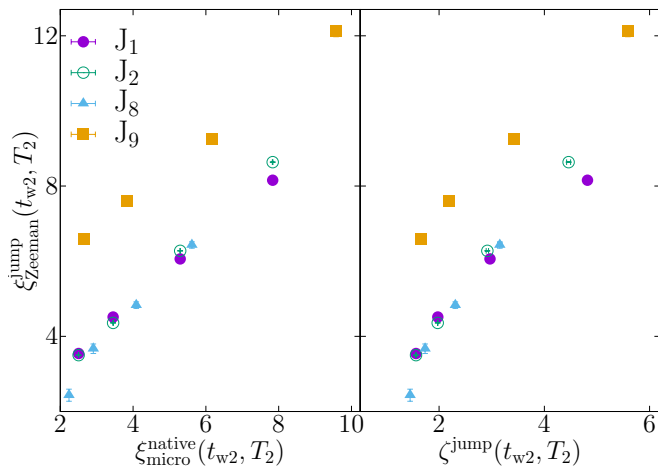


FIG. 5. **Comparison between correlation lengths.** Left: we compare the behavior of the effective correlation length, $\xi_{\text{Zeeman}}^{\text{jump}}$, as a function of the microscopic correlation length, $\xi_{\text{micro}}^{\text{native}}(t_{w2}, T_2)$ evaluated at a fixed-temperature. Right: we show the behavior of $\xi_{\text{Zeeman}}^{\text{jump}}$ as a function of the coherence scale $\zeta(t_{w2}, T_2)$ calculated for varying-temperatures. The J_n temperature cycles and related wait times t_{w1} are listed in Table II in the main text.

but are otherwise statistically independent). Replicas are employed to compute correlation functions as explained in Refs. [19, 20, 30]

Appendix B: A simple relation between coherence lengths

In this section we define the relevant length scales, ξ_{micro} , ζ and ξ_{Zeeman} and their relationships:

- $\xi_{\text{micro}}(t_w)$ is the size of the glassy domain. It is estimated through the replicon propagator, $G_{\text{R}}(r, t_w; p)$.
- ξ_{Zeeman} is obtained by counting the number of spins that react coherently to an external magnetic field, and thereby the volume of correlated spins subtended by the correlation length ξ_{Zeeman} . This is the only experimentally accessible method for obtaining a correlation length directly.
- $\zeta(t_1, t_2)$ is the scale at which defects are correlated [51].

In a fixed-temperature protocol, these quantities are almost equivalent [19, 20, 30]. The scenario is more intricate in varying-temperature protocols because of temperature chaos. In Fig. 5, we compare these length scales in varying-temperature protocols.

As the reader can notice, if chaos is large [J_1 , J_2 and J_8], an equivalence exists between ξ_{Zeeman} , ζ , and ξ_{micro} . Otherwise [J_9], the number of correlated spins is not a good proxy for ζ .

Appendix C: Scaling of χ' , χ'' and χ_2/V

In this section, we show that the dynamical behavior of the three susceptibilities, χ' , χ'' and $\hat{\chi}_2 \equiv \chi_2/V$, are similar. The former two are measured in conventional memory experiments (*e.g.*, in Ref. [35]), and the latter in numerical simulations.

We analyze first the scaling properties near the critical point. We then extend the analysis to the glass phase.

In the following we use $\epsilon \equiv (T - T_g)/T_g$ to denote the reduced temperature.

On the one hand, the experimentally computed *linear* magnetic susceptibilities behave as [47]

$$\begin{aligned} \frac{\chi_0 - \chi'}{\chi_0} &\sim \epsilon^\beta G(t/\tau), \\ \chi'' &\sim \epsilon^\beta H(t/\tau), \end{aligned} \quad (\text{C1})$$

where we have taken both linear magnetic susceptibilities in the time domain (the relationship to frequency is a simple Fourier transform). Above, $G(\cdot)$ and $H(\cdot)$ are two scaling functions, and χ_0 is the equilibrium value of the linear magnetic susceptibility at the critical point.

On the other hand, the *nonlinear* spin-glass susceptibility per spin, computed in numerical simulations, scales as [47]

$$\hat{\chi}_2 \sim \epsilon^{2\beta} K(t/\tau), \quad (\text{C2})$$

with a suitable scaling function $K(\cdot)$. At the critical point, there is only a critical mode and we can avoid the use of the replicon term.

The rationale behind these scaling relations is that the overlap is essentially the magnetization squared. The linear magnetic susceptibilities scale with the exponent associated with the average of the overlap q (the fluctuation of the magnetization is given by $\langle m^2 \rangle$, the average of the overlap), and χ_2 is a nonlinear susceptibility per spin associated with the overlap. Therefore, it scales with the usual exponent $\gamma = 2\beta - \nu D$. Remember that the order parameter, the overlap, scales with the exponent β and that $\hat{\chi}_2 = \chi_2/V$.

For the analogous scaling relations in the spin-glass phase, the out-of-equilibrium situation is dominated by the replicon mode. The only diverging nonlinear susceptibility is the replicon nonlinear one, defined as

$$\chi_2(t) = \int_0^\infty dr r^2 G_{\text{R}}(r, t). \quad (\text{C3})$$

The overlap field scales with the replicon exponent θ as $q \sim \xi^{-\theta/2}$ (see Appendix H of [46]), so we can write the dependence of these susceptibilities on the correlation length as

$$\begin{aligned} \frac{\chi_0 - \chi'}{\chi_0} &\sim \chi'' \sim \xi(t)^{-\theta/2}, \\ \hat{\chi}_2 &\sim \xi(t)^{-\theta}. \end{aligned} \quad (\text{C4})$$

We conclude from this analysis that the dynamical behaviors of these different susceptibilities are similar. Hence, we can safely compare the results from numerical simulations with experiments that measure χ'' [35] for this reason.

Appendix D: Experimental details and data processing

This section explores the experimental protocol for measuring the change in magnetization as a function of $\log t$. In particular, it delves into the nuances of data processing for accurate identification of the time that the dynamic function $S(t)$ peaks, $t_w^{\text{eff}}(H)$. As discussed in the main body of the text, the accurate determination of $t_w^{\text{eff}}(H)$ is vital for extracting ξ_{Zeeman} .

Magnetization measurements were conducted using a Quantum Design MPMS system. The magnetization was gauged as the sample traversed through an array of superconducting quantum interference devices (SQUIDs). The system was set to take continuous magnetization measurements over approximately 10 hours for $t_w = 1$ h, and 30 hours for $t_w = 3$ h.

The magnetization as a function of time t displayed intermittent spikes owing to the SQUIDs' measurements. A representative example is exhibited in Figure 6. These aberrations, typically because of external interference with the SQUID coil, were subsequently removed in our analysis. The first derivative of the magnetization as a function of $\log t$ was then calculated.

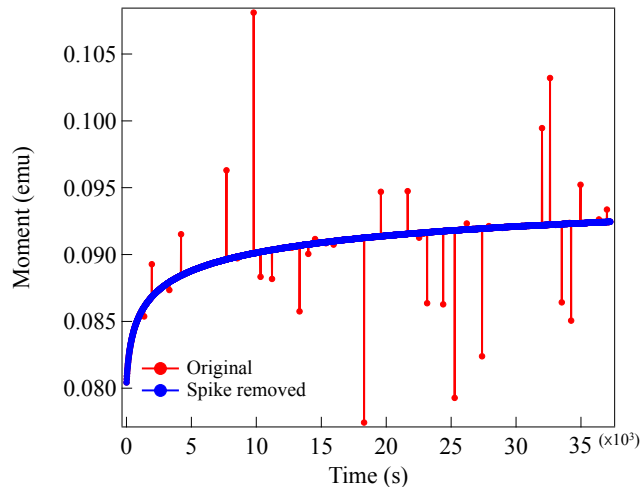


FIG. 6. **Raw measurement data and the spike removed data** Data from a typical $S(t)$ measurement. (Red) The raw magnetization vs t with random spikes from the SQUID measurements. (Blue) Magnetization vs t with spikes removed.

The derivative of the raw data tends to be noisy, complicating the task of identifying the position of the peak in $S(t)$. It was necessary to suitably smooth the $S(t)$

curve. We utilized a Chebyshev polynomial fit for the M vs t curve prior to computing its derivative.

With an appropriate number of terms, the Chebyshev polynomial fit accurately represents the raw M vs t data, effectively eliminating the spikes in the $dM/d\log t$ data produced by measurement artifacts, as illustrated in Figure 7. A 60-term Chebyshev polynomial fit typically depicts the $S(t)$ curve satisfactorily, with less than a 1% residual. Using higher terms further reduces this residual. The Chebyshev polynomial fit excels over a simple box smoothing of raw data because it preserves the spline of the M vs t curve while simultaneously decreasing the noise in the derivative.

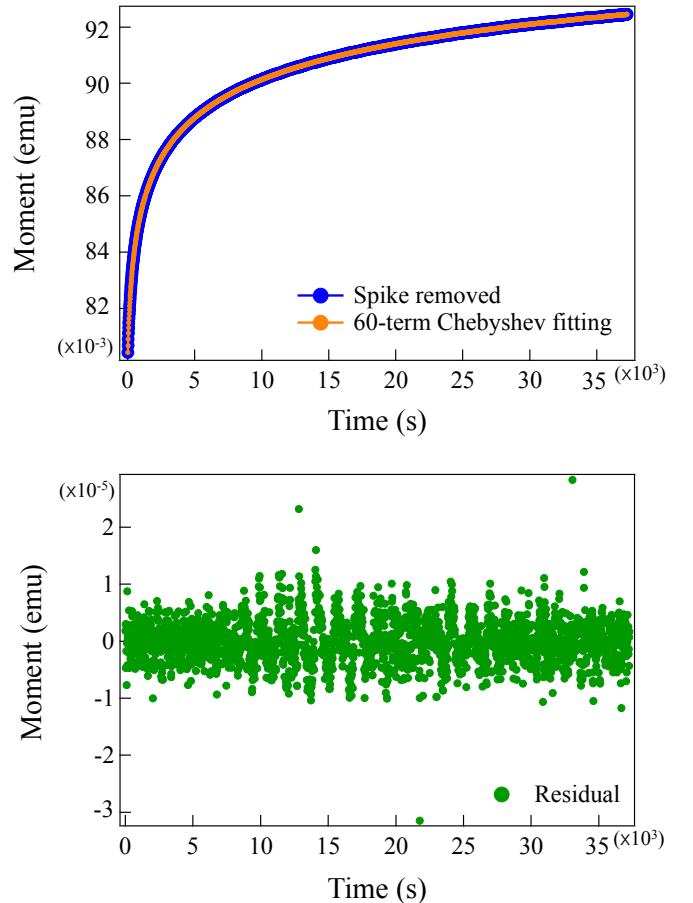


FIG. 7. **Chebyshev polynomial fitting of the data and the residual** (Top) The spike removed M vs t data with 60-term Chebyshev fit of the data marked in orange. (Bottom) The residual of the Chebyshev fit.

Upon obtaining the derivative of the Chebyshev polynomial, we constructed a single Lorentzian peak function with a constant background:

$$f(x) = \frac{A\gamma^2}{(x - x_0)^2 + \gamma^2} + C \quad . \quad (\text{D1})$$

In this equation, A denotes the amplitude of the peak, x_0 represents the center, and γ indicates the peak width.

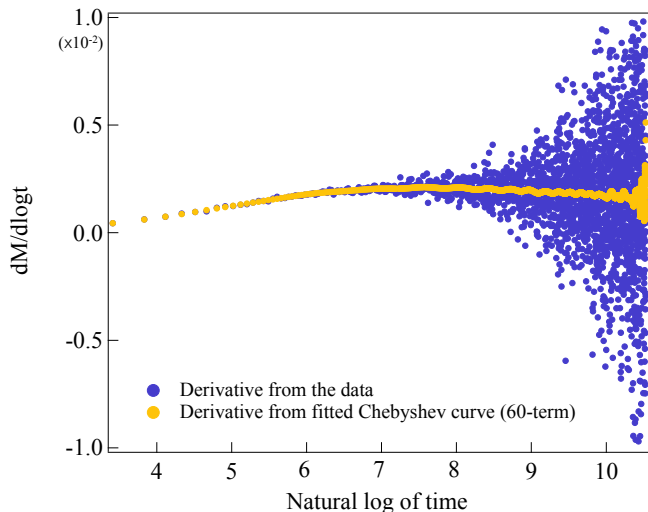


FIG. 8. **Comparison of the derivative of the raw data vs the derivative of one Chebyshev fitted curve.** (Blue) The $dM/d \log t$ plot of raw magnetization vs $\log t$. (Yellow) The $dM/d \log t$ plot of a 60-term Chebyshev fit of the magnetization vs $\log t$.

As depicted in Figure 8, the derivative of the Chebyshev curve provides a relatively uncluttered peak with a fit to a Lorentzian shape. With a sufficient number of Chebyshev polynomial terms, the fitted curve can trace the raw data precisely.

To ensure that the Chebyshev polynomial accurately represents the M vs t data, we iteratively conducted the fitting and peak searching procedure over a number range of terms, typically from 30 to 1200. Each iteration produced a value for the time at which the Lorentzian peaks. We then calculated the average of these values to deter-

mine the peak time for a given $S(t)$ measurement. The error bar for the time of the peak was determined from the standard deviation of the peak times. In cases where overfitting or underfitting was apparent within certain ranges of the number of Chebyshev polynomial terms, as evinced by deviant peak values, the peak values obtained in these ranges were disregarded.

Appendix E: Determination of the coefficients for the scaling function $\mathcal{F}(x, y)$

As we have explained in the main text, we introduce a simple scaling function $\mathcal{F}(x, y)$ for describing both the experimental and numerical data. Here we report the details for the determination of the constants a_1 and a_2 [and analogously a'_1 and a'_2].

Our procedure consists of two steps:

- we fit the data for the memory coefficient under consideration — \mathcal{C}_{num} or $\mathcal{C}_{\chi''}$ — to a smooth, generic function of the scaling function $\mathcal{F}(x, y)$ introduced in the main text[52]:

$$\mathcal{C}(x, y) = B_0 - B_1 \mathcal{F}(x, y) - B_2 [\mathcal{F}(x, y)]^2, \quad (\text{E1})$$

Note that there are five fit parameters, namely B_0 , B_1 and B_2 and the two parameters a_1 and a_2 that determine $\mathcal{F}(x, y)$.

- The free parameters B_0, B_1, B_2 are disregarded in the analysis. Instead, we keep a_1, a_2 (or a'_1 and a'_2 for $\mathcal{C}_{\chi''}$), to describe our data as a function of the scaling function $\mathcal{F}(x, y)$ [$\mathcal{F}'(x', y')$ in the case of $\mathcal{C}_{\chi''}$].

For the numerical data, $B_0 \simeq 1$ and $B_2 = 0$. The data for $\mathcal{C}_{\chi''}$, taken from Ref. [35], require $B_2 \neq 0$.

-
- [1] N. C. Keim, J. D. Paulsen, Z. Zeravcic, S. Sastry, and S. R. Nagel, *Rev. Mod. Phys.* **91**, 035002 (2019).
- [2] M. M. Bandi, H. G. E. Hentschel, I. Procaccia, S. Roy, and J. Zylberg, *Europhys. Lett.* **122**, 38003 (2018).
- [3] T. Koide, G. Krein, and R. O. Ramos, *Phys. Lett. B* **636**, 96 (2006).
- [4] F. Ozon, T. Narita, A. Knaebel, P. Debrégeas, Hébraud, and J.-P. Munch, *Phys. Rev. E* **68**, 032401 (2003).
- [5] L. Bellon, S. Ciliberto, and C. Laroche, *Europhys. Lett.* **51**, 551 (2000).
- [6] H. Yardimci and R. L. Leheny, *Europhys. Lett.* **62**, 203 (2003).
- [7] J.-P. Bouchaud, P. Doussineau, T. de Lacerda-Arôso, and A. Levelut, *Eur. Phys. J. B* **21**, 335 (2001).
- [8] V. Mueller and Y. Shchur, *Europhys. Lett.* **65**, 137 (2004).
- [9] C. Scalliet and L. Berthier, *Phys. Rev. Lett.* **122**, 255502 (2019).
- [10] N. Pashine, D. Hexner, A. J. Liu, and S. R. Nagel, *Science Advances* **5**, eaax4215 (2019), <https://www.science.org/doi/pdf/10.1126/sciadv.aax4215>.
- [11] F. Lefloch, J. Hammann, M. Ocio, and E. Vincent, *EPL (Europhysics Letters)* **18**, 647 (1992).
- [12] K. Jonason, E. Vincent, J. Hammann, J. P. Bouchaud, and P. Nordblad, *Phys. Rev. Lett.* **81**, 3243 (1998).
- [13] L. Lundgren, P. Svedlindh, and O. Beckman, *J. Magn. Mater.* **31–34**, 1349 (1983).
- [14] T. Jonsson, K. Jonason, P. E. Jönsson, and P. Nordblad, *Phys. Rev. B* **59**, 8770 (1999).
- [15] J. Hammann, E. Vincent, V. Dupuis, M. Alba, M. Ocio, and J.-P. Bouchaud, *J. Phys. Soc. Jpn.*, Suppl A. 206 (2000).
- [16] E. Vincent, in *Ageing and the Glass Transition*, Lecture Notes in Physics No. 716, edited by M. Henkel, M. Pleimling, and R. Sanctuary (Springer, 2007).
- [17] E. Vincent, “Spin glass experiments,” (2023), to appear in Elsevier Encyclopedia of Condensed Matter Physics, 2nd ed., [arXiv:2208.00981](https://arxiv.org/abs/2208.00981).

- [18] Q. Zhai, V. Martin-Mayor, D. L. Schlagel, G. G. Kenning, and R. L. Orbach, *Phys. Rev. B* **100**, 094202 (2019).
- [19] Q. Zhai, I. Paga, M. Baity-Jesi, E. Calore, A. Cruz, L. A. Fernandez, J. M. Gil-Narvion, I. Gonzalez-Adalid Pemarkin, A. Gordillo-Guerrero, D. Iñiguez, A. Maiorano, E. Marinari, V. Martin-Mayor, J. Moreno-Gordo, A. Muñoz Sudupe, D. Navarro, R. L. Orbach, G. Parisi, S. Perez-Gaviro, F. Ricci-Tersenghi, J. J. Ruiz-Lorenzo, S. F. Schifano, D. L. Schlagel, B. Seoane, A. Tarancon, R. Tripiccion, and D. Yllanes, *Phys. Rev. Lett.* **125**, 237202 (2020).
- [20] I. Paga, Q. Zhai, M. Baity-Jesi, E. Calore, A. Cruz, L. A. Fernandez, J. M. Gil-Narvion, I. Gonzalez-Adalid Pemarkin, A. Gordillo-Guerrero, D. Iñiguez, A. Maiorano, E. Marinari, V. Martin-Mayor, J. Moreno-Gordo, A. Muñoz-Sudupe, D. Navarro, R. L. Orbach, G. Parisi, S. Perez-Gaviro, F. Ricci-Tersenghi, J. J. Ruiz-Lorenzo, S. F. Schifano, D. L. Schlagel, B. Seoane, A. Tarancon, R. Tripiccion, and D. Yllanes, *Journal of Statistical Mechanics: Theory and Experiment* **2021**, 033301 (2021).
- [21] M. Baity-Jesi, E. Calore, A. Cruz, L. A. Fernandez, J. M. Gil-Narvion, A. Gordillo-Guerrero, D. Iñiguez, A. Maiorano, E. Marinari, V. Martin-Mayor, J. Moreno-Gordo, A. Muñoz Sudupe, D. Navarro, G. Parisi, S. Perez-Gaviro, F. Ricci-Tersenghi, J. J. Ruiz-Lorenzo, S. F. Schifano, B. Seoane, A. Tarancon, R. Tripiccion, and D. Yllanes (Janus Collaboration), *Phys. Rev. Lett.* **120**, 267203 (2018).
- [22] M. Baity-Jesi, E. Calore, A. Cruz, L. A. Fernandez, J. M. Gil-Narvion, I. Gonzalez-Adalid Pemarkin, A. Gordillo-Guerrero, D. Iñiguez, A. Maiorano, E. Marinari, V. Martin-Mayor, J. Moreno-Gordo, A. Muñoz Sudupe, D. Navarro, I. Paga, G. Parisi, S. Perez-Gaviro, F. Ricci-Tersenghi, J. J. Ruiz-Lorenzo, S. F. Schifano, B. Seoane, A. Tarancon, R. Tripiccion, and D. Yllanes, *Communications physics* **4**, 74 (2021), <https://www.nature.com/articles/s42005-021-00565-9.pdf>.
- [23] Q. Zhai, R. L. Orbach, and D. L. Schlagel, *Phys. Rev. B* **105**, 014434 (2022).
- [24] T. Komori, H. Yoshino, and H. Takayama, *Journal of the Physical Society of Japan* **69**, 1192 (2000), [arXiv:cond-mat/9908078](https://arxiv.org/abs/cond-mat/9908078).
- [25] M. Picco, F. Ricci-Tersenghi, and F. Ritort, *Phys. Rev. B* **63**, 174412 (2001).
- [26] L. Berthier and J.-P. Bouchaud, *Phys. Rev. B* **66**, 054404 (2002).
- [27] H. Takayama and K. Hukushima, *Journal of the Physical Society of Japan* **71**, 3003 (2002).
- [28] A. Maiorano, E. Marinari, and F. Ricci-Tersenghi, *Phys. Rev. B* **72**, 104411 (2005).
- [29] S. Jiménez, V. Martín-Mayor, and S. Pérez-Gaviro, *Phys. Rev. B* **72**, 054417 (2005).
- [30] M. Baity-Jesi, E. Calore, A. Cruz, L. A. Fernandez, J. M. Gil-Narvion, I. Gonzalez-Adalid Pemarkin, A. Gordillo-Guerrero, D. Iñiguez, A. Maiorano, E. Marinari, V. Martin-Mayor, J. Moreno-Gordo, A. Muñoz Sudupe, D. Navarro, I. Paga, G. Parisi, S. Perez-Gaviro, F. Ricci-Tersenghi, J. J. Ruiz-Lorenzo, S. F. Schifano, B. Seoane, A. Tarancon, and D. Yllanes, *Nat. Phys.* (2023), <https://doi.org/10.1038/s41567-023-02014-6>, [arXiv:2207.06207](https://arxiv.org/abs/2207.06207).
- [31] M. Baity-Jesi, R. A. Baños, A. Cruz, L. A. Fernandez, J. M. Gil-Narvion, A. Gordillo-Guerrero, D. Iniguez, A. Maiorano, F. Mantovani, E. Marinari, V. Martín-Mayor, J. Monforte-Garcia, A. Muñoz Sudupe, D. Navarro, G. Parisi, S. Perez-Gaviro, F. Ricci-Tersenghi, J. J. Ruiz-Lorenzo, S. F. Schifano, B. Seoane, A. Tarancon, R. Tripiccion, and D. Yllanes (Janus Collaboration), *Comp. Phys. Comm* **185**, 550 (2014), [arXiv:1310.1032](https://arxiv.org/abs/1310.1032).
- [32] L. A. Fernandez, V. Martín-Mayor, G. Parisi, and B. Seoane, *EPL* **103**, 67003 (2013), [arXiv:1307.2361](https://arxiv.org/abs/1307.2361).
- [33] L. A. Fernández, E. Marinari, V. Martín-Mayor, G. Parisi, and D. Yllanes, *Journal of Statistical Mechanics: Theory and Experiment* **2016**, 123301 (2016), [arXiv:1605.03025](https://arxiv.org/abs/1605.03025).
- [34] A. Billoire, L. A. Fernandez, A. Maiorano, E. Marinari, V. Martin-Mayor, J. Moreno-Gordo, G. Parisi, F. Ricci-Tersenghi, and J. J. Ruiz-Lorenzo, *Journal of Statistical Mechanics: Theory and Experiment* **2018**, 033302 (2018).
- [35] J. Freedberg, W. J. Meese, J. He, D. L. Schlagel, E. D. Dahlberg, and R. L. Orbach, “On the nature of memory and rejuvenation in glassy systems,” (2023), [arXiv:2305.17296](https://arxiv.org/abs/2305.17296) [cond-mat.dis-nn].
- [36] I. Paga, Q. Zhai, M. Baity-Jesi, E. Calore, A. Cruz, C. Cummings, L. A. Fernandez, J. M. Gil-Narvion, I. G.-A. Pemarkin, A. Gordillo-Guerrero, D. Iñiguez, G. G. Kenning, A. Maiorano, E. Marinari, V. Martin-Mayor, J. Moreno-Gordo, A. Muñoz Sudupe, D. Navarro, R. L. Orbach, G. Parisi, S. Perez-Gaviro, F. Ricci-Tersenghi, J. J. Ruiz-Lorenzo, S. F. Schifano, D. L. Schlagel, B. Seoane, A. Tarancon, and D. Yllanes, *Phys. Rev. B* **107**, 214436 (2023).
- [37] See Supplemental Material [url], which includes Refs. [49, 50] for details.
- [38] Y. G. Joh, R. Orbach, G. G. Wood, J. Hammann, and E. Vincent, *Phys. Rev. Lett.* **82**, 438 (1999).
- [39] F. Belletti, M. Cotallo, A. Cruz, L. A. Fernandez, A. Gordillo-Guerrero, M. Guidetti, A. Maiorano, F. Mantovani, E. Marinari, V. Martín-Mayor, A. M. Sudupe, D. Navarro, G. Parisi, S. Perez-Gaviro, J. J. Ruiz-Lorenzo, S. F. Schifano, D. Sciretti, A. Tarancon, R. Tripiccion, J. L. Velasco, and D. Yllanes (Janus Collaboration), *Phys. Rev. Lett.* **101**, 157201 (2008), [arXiv:0804.1471](https://arxiv.org/abs/0804.1471).
- [40] F. Belletti, A. Cruz, L. A. Fernandez, A. Gordillo-Guerrero, M. Guidetti, A. Maiorano, F. Mantovani, E. Marinari, V. Martín-Mayor, J. Monforte, A. Muñoz Sudupe, D. Navarro, G. Parisi, S. Perez-Gaviro, J. J. Ruiz-Lorenzo, S. F. Schifano, D. Sciretti, A. Tarancon, R. Tripiccion, and D. Yllanes (Janus Collaboration), *J. Stat. Phys.* **135**, 1121 (2009), [arXiv:0811.2864](https://arxiv.org/abs/0811.2864).
- [41] M. Baity-Jesi, E. Calore, A. Cruz, L. A. Fernandez, J. M. Gil-Narvion, A. Gordillo-Guerrero, D. Iñiguez, A. Maiorano, E. Marinari, V. Martin-Mayor, J. Monforte-Garcia, A. Muñoz Sudupe, D. Navarro, G. Parisi, S. Perez-Gaviro, F. Ricci-Tersenghi, J. J. Ruiz-Lorenzo, S. F. Schifano, B. Seoane, A. Tarancon, R. Tripiccion, and D. Yllanes, *Proceedings of the National Academy of Sciences* **114**, 1838 (2017).
- [42] Our simulations will closely follow [30] (for the sake of completeness we describe them in Table II and in the Supplemental Materials).
- [43] Due to rotational invariance [40], G_R essentially depends on $r = |\mathbf{r}|$.

- [44] M. Baity-Jesi, E. Calore, A. Cruz, L. A. Fernandez, J. M. Gil-Narvion, A. Gordillo-Guerrero, D. Iñiguez, A. Maiorano, E. Marinari, V. Martin-Mayor, J. Monforte-Garcia, A. Muñoz Sudupe, D. Navarro, G. Parisi, S. Perez-Gaviro, F. Ricci-Tersenghi, J. J. Ruiz-Lorenzo, S. F. Schifano, B. Seoane, A. Tarancon, R. Tripiccion, and D. Yllanes (Janus Collaboration), *Phys. Rev. Lett.* **118**, 157202 (2017).
- [45] A native protocol can be regarded as a cycle with $t_{w2} = t_{w3} = 0$ ($t_{w1} + 2^{10}$ is indistinguishable from t_{w1} within our numerical accuracy for native runs).
- [46] L. A. Fernandez, I. Gonzalez-Adalid Pemartin, V. Martin-Mayor, G. Parisi, F. Ricci-Tersenghi, T. Rizzo, J. J. Ruiz-Lorenzo, and M. Veca, *Phys. Rev. E* **105**, 054106 (2022).
- [47] P. Nordblad and P. Svedlindh, *Experiments on Spin Glasses* (World Scientific, Singapore, 1997) spin Glasses and Random Fields edited by A.P. Young, Directions in Condensed Matter Physics Vol. 12, p. 1.
- [48] We computed x' and y' from the approximation $\zeta(T_2, t_{w2}) \approx \xi_{\text{micro}}(T_2, t_{w2})$ [30] and the approximate law $\xi_{\text{micro}}(T, t_w)/a \approx 0.58(t/t_w)^{c_2 T/T_g}$ with $c_2 = 0.104$ and $\tau = 0.186$ ps [18]. Indeed, our measurements of ξ in Table I rather follow $\xi/a \approx 0.58(t/t_w)^{c_2 T/T_g} + 3.9$. We omit the constant background 3.9 to diminish corrections to scaling.
- [49] M. Baity-Jesi, R. A. Baños, A. Cruz, L. A. Fernandez, J. M. Gil-Narvion, A. Gordillo-Guerrero, D. Iniguez, A. Maiorano, F. Mantovani, E. Marinari, V. Martín-Mayor, J. Monforte-Garcia, A. Muñoz Sudupe, D. Navarro, G. Parisi, S. Perez-Gaviro, M. Pivanti, F. Ricci-Tersenghi, J. J. Ruiz-Lorenzo, S. F. Schifano, B. Seoane, A. Tarancon, R. Tripiccion, and D. Yllanes (Janus Collaboration), *Phys. Rev. B* **88**, 224416 (2013), arXiv:1310.2910.
- [50] J. A. Mydosh, *Spin Glasses: an Experimental Introduction* (Taylor and Francis, London, 1993).
- [51] See Refs. [30, 39] for more details.
- [52] We employ $\mathcal{F}(x, y)$ for C_{num} and $\mathcal{F}'(x', y')$ for $C_{\chi''}$.